Whistler Mode Wave Refractive Index in a Finite Temperature Anisotropic Plasma Medium

Marek Gołkowski
Department of Electrical Engineering
University of Colorado Denver
Denver, CO USA
mark.golkowski@ucdenver.edu

Ashanthi Maxworth
Institute of Space and Atmospheric Studies
Department of Physics and Engineering Physics
University of Saskatchewan
Saskatoon, SK, Canada
asm468@mail.usask.ca

***Abstract*—Whistler mode waves, which exist in a magnetized plasma, are prevalent in the Earth's magnetosphere in the extremely low frequency (ELF) and very low frequency (VLF) bands (100 Hz - 30 kHz). Due to the impact of whistler mode waves on space weather processes, it is important to accurately predict the propagation trajectory of these waves and their properties. Numerical raytracing determines the power flow path of the whistler mode waves in the anisotropic medium of the magnetosphere based on local calculation of the refractive index. In the majority of previous work, magnetospheric raytracing has been implemented assuming a cold background plasma (0 K). However, a more accurate description of the magnetospheric plasma includes a background temperature of about 1 eV (11600 K). We present solutions to the dispersion relation that include the effects of finite electron and ion temperatures on the wave refractive index using a warm plasma formulation. Finite temperature effects of the background plasma are shown to be most significant for highly oblique wave normal angles where the refractive index is bounded to smaller values than in the ideal cold plasma approximation.**

Keywords—*oblique whistler waves, radiation belts, raytracing, warm plasma, whistler mode*.

I. Introduction

Whistler mode waves are electromagnetic plasma waves that exists in a magnetized plasma, typically with plasma frequency much greater than electron cyclotron frequency. They are characterized by group and phase velocities much less than the speed of light with significant dispersion and a polarization that is generally right hand elliptically polarized [1]. Whistler mode waves are prominent in certain laboratory plasma applications and also play a key role in the energy dynamics of the near-Earth space environment, which we focus on here. Due to the plasma medium therein and the dominant effect of the geomagnetic field, this region is termed the magnetosphere and hosts a variety of whistler mode waves from diverse sources including manmade transmitters, atmospheric lightning, and local plasma instabilities. The medium is highly anisotropic making the prediction of wave trajectories analytically intractable outside of special cases. The power flow path of whistler mode waves can be determined using numerical raytracing. The magnetosphere contains two distinct populations of plasma, the background low temperature plasma with densities of 1 - 5000 cm^{-3} and a much smaller population of hot plasma with densities below 1 cm^{-3} but energies in the 10 keV – 1 MeV range. (The hot plasma population is often called the radiation belts.) The hot plasma drives instabilities, but the background low temperature plasma determines the propagation characteristics of waves. The majority of the previous work on magnetospheric raytracing was performed assuming an ideally cold background plasma. However, observations show that the magnetospheric background exhibits finite temperatures of around 1 eV or greater [2]. In this work we investigate how refractive index surfaces change with the inclusion of finite background temperature to electrons and ions. Finite temperature effects become important for highly oblique whistler mode waves. For highly oblique waves near the resonance cone (limit of cold plasma solutions), the warm plasma formulations can be approximated by quasi-electrostatic or electrostatic models for frequencies below the half cyclotron frequency but at higher frequencies the models diverge. The results suggest that warm plasma raytracing codes are able to capture the important wave characteristics for all wave normal angles and are therefore more robust than quasi-electrostatic assumptions and not significantly more computationally expensive than cold plasma raytracing.

II. Warm Plasma Model

A. Refractive Index Surfaces

Numerical ray tracing is the process of determining the power flow path of a whistler wave by solving the Haselgrove equations [3] under a WKB assumption. The medium properties enter the formulation through the refractive index, μ, which is a strong function of wave normal angle θ, which is the angle between the wave normal vector and the geomagnetic field. Under the ideal cold plasma assumption the dispersion relation is fourth order in μ:

$$A_0\mu^4 + B_0\mu^2 + C_0 = 0, \tag{1}$$

where the parameters A_0, B_0, and C_0 are cold plasma parameters defined below [4,5]. With the inclusion of finite temperature, the dispersion relation becomes sixth order:

$$q^T A_1\ \mu^6\left(A_0 + q^T B_1\right)\mu^4 + \left(B_0 + q^T C_1\right)\mu^2 + C_0 = 0, \tag{2}$$

where temperature T_s of each plasma species, *s*, is captured in:

Submitted On: September 30, 2018
Accepted On: October 3, 2018

$$q_s^T = \frac{k_B T_s}{m_s c^2}. \quad (3)$$

Where k_B is the Boltzmann constant, m_s is the mass and c is the speed of light. Since in most cases $q^T A_1 << A_0$, the first term in (2) only becomes significant in cases where μ is large. This occurs for highly oblique wave normal angles near the so called resonance cone for which the cold plasma assumption yields $\mu \to \infty$. If more than one plasma species (i.e., electron and ions) has finite temperature, then (1) becomes a summation over the species s:

$$(\sum_s q_s{}^T A_{1s})\mu^6 + (A_0 + \sum_s q_s{}^T B_{1s})\mu^4 + (B_0 + \sum_s q_s{}^T C_{1s})\mu^2 + C_0 = 0. \quad (4)$$

The remaining parameters are defined below. The dielectric tensor can be defined as having a cold and warm component:

$$\boldsymbol{K} = \boldsymbol{K^0} + \boldsymbol{\tau K^1}.$$

The elements of the cold tensor $\boldsymbol{K^0}$ are the well-known formulations from magneto-ionic theory:

$$\boldsymbol{K^0} = \begin{bmatrix} 1 - \frac{X}{1-Y^2} & \frac{iXY}{1-Y^2} & 0 \\ \frac{-iXY}{1-Y^2} & 1 - \frac{X}{1-Y^2} & 0 \\ 0 & 0 & 1-X \end{bmatrix},$$

$$X_s = \frac{\omega_{ps}{}^2}{\omega^2},$$

$$Y_s = \frac{\omega_{cs}}{\omega},$$

where ω is the wave frequency and ω_{ps} and ω_{cs} are the plasma frequency and cyclotron frequency, respectively for each particle species. The element of the finite temperature tensor $\boldsymbol{K^1}$ tensor are:

$$K_{11s}{}^1 = \frac{-X_s}{1-Y_s{}^2}\left[\frac{3sin^2\theta}{1-4Y_s{}^2} + \frac{1+3Y_s{}^2}{(1-Y_s{}^2)^2}cos^2\theta\right],$$

$$K_{22s}{}^1 = \frac{-X_s}{1-Y_s{}^2}\left[\frac{1+8Y_s{}^2}{1-4Y_s{}^2}sin^2\theta + \frac{1+3Y_s{}^2}{(1-Y_s{}^2)^2}cos^2\theta\right],$$

$$K_{33s}{}^1 = -X_s\left[3cos^2\theta + \frac{sin^2\theta}{1-Y_s{}^2}\right],$$

$$K_{12s}{}^1 = -K_{21s}{}^1 = \frac{iX_sY_s}{1-Y_s{}^2}\left[\frac{6sin^2\theta}{1-4Y_s{}^2} + \frac{3+Y_s{}^2}{(1-Y_s{}^2)^2}cos^2\theta\right],$$

$$K_{23s}{}^1 = -K_{32s}{}^1 = \frac{-iX_sY_s}{(1-Y_s{}^2)^2}(3-Y_s{}^2).sin\theta.cos\theta,$$

$$K_{13s}{}^1 = K_{31s}{}^1 = \frac{-2X_s}{(1-Y_s{}^2)^2}.sin\theta.cos\theta.$$

From the tensor components, the coefficients in (4) can be defined as:

$$A_0 = K_{11}{}^0 sin^2\theta + K_{33}{}^0 cos^2\theta,$$

$$B_0 = -[K_{11}{}^0.K_{22}{}^0 + (K_{12}{}^0)^2].sin^2\theta - K_{33}{}^0[K_{11}{}^0 + K_{22}{}^0.cos^2\theta],$$

$$C_0 = K_{33}{}^0\left[(K_{12}{}^0)^2 + K_{11}{}^0.K_{22}{}^0\right],$$

$$A_{1s} = K_{11s}{}^1 sin^2\theta + K_{33s}{}^1 cos^2\theta + 2K_{13s}{}^1.sin\theta.cos\theta,$$

$$B_{1s} = -[K_{11s}{}^1.K_{22}{}^0 + K_{22s}{}^1.K_{11}{}^0 + 2K_{12}{}^0.K_{12s}{}^1].sin^2\theta - K_{33s}{}^1[K_{11}{}^0 + K_{22}{}^0.cos^2\theta] - K_{33}{}^0[K_{11s}{}^1 + K_{22s}{}^1.cos^2\theta] + 2.sin\theta.cos\theta.[K_{12}{}^0.K_{23s}{}^1 - K_{13s}{}^1.K_{22}{}^0],$$

$$C_{1s} = K_{33s}{}^1\left[(K_{12}{}^0)^2 + K_{11}{}^0.K_{22}{}^0\right] + K_{33}{}^0[2K_{12}{}^0.K_{12s}{}^1 + K_{11}{}^0.K_{22s}{}^1 + K_{11s}{}^1.K_{22}{}^0].$$

Details of derivation of above expressions are provided in [4, 5] and references therein. Fig. 1 shows the refractive index surface for an example case of 3 kHz wave at the geomagnetic equator two Earth radii from the surface (L = 2) for various electron and ion temperatures as well as the cold plasma case. It is seen that the finite temperature effects cause the refractive index surface to deviate from the cold plasma value only for highly oblique angles near the resonance cone. The magnitude of refractive index is seen to decrease with temperature.

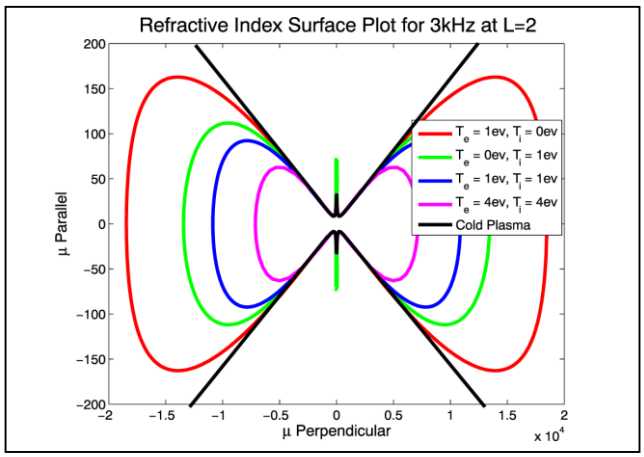

Fig. 1. Refractive index surfaces at the magnetic equator for the cold plasma and finite temperatures for ions and electrons. The refractive indeex is "open" under the cold plasma assumption but closed surfaces when temperature effects are included [5]. Note the disparate scale of the vertical and horizontal axes. The resonance cone angle is 89.1°.

III. Comparison with Quasi-electrostatic and Electrostatic Approximations

There has recently been interest in estimating the refractive index for highly oblique whistler mode waves where cold plasma theory is inadequate. Ma *et al.* [6] have employed a quasi-electrostatic assumption and shown reasonable

Work was supported by the National Science Foundation grants AGS 1254365 and AGS 1451210 to University of Colorado Denver.

agreement with spacecraft observations. We perform a comparison of refractive index values obtained under warm plasma assumptions, quasi electrostatic and electrostatic assumptions. Quasi-electrostatic and electrostatic refractive index models of whistler mode refractive index have been presented by *Horne and Sazhin* [8]. In that work two plasma populations were considered: a finite temperature background plasma at 1 eV and a smaller hot plasma population at 200 eV. In the electrostatic and quasi-electrostatic simplified models of *Horne and Sazhin* [8], the two plasma populations each contribute to the refractive index calculation. The warm plasma formulations presented here take the more traditional approach from whistler mode raytracing where the background plasma determines the refractive index and wave trajectory and a hot plasma distribution can later be introduced to calculate resonance effects like wave growth or damping. For this reason and due to the fact that the hot plasma of the radiation belts is very dynamic and hard to generalize, we perform comparisons of the models using the background 1 eV plasma only. Figs. 2-7 present the comparison results obtained from the above three methods, at the equator at $L = 4, 6$ and 6.6, and for two frequencies normalized to the local cyclotron frequency with ratios ω/ω_c of 0.4 and 0.6. The three locations were selected as just-inside the plasma-pause ($L=4$) with background density N_e = 200 cm^{-3}, outside the plasma pause ($L=6$) with density N_e = 8.5 cm^{-3}and at the geostationary orbit ($L=6.6$) with density N_e = 1 cm^{-3}. At all locations the electron and ion temperature is T_e =T_i = 1 eV. The three gyro-frequencies corresponding to the equator of $L = 4, 6$ and 6.6 are 12 kHz, 4 kHz and 3 kHz respectively. The electrostatic and quasi electrostatic models are parametrized with the value λ given in (5) as the ratio between the squared sum of background electron plasma frequency and the squared electron gyro-frequency:

$$\lambda = \frac{\omega_p^2}{\omega_c^2}. \tag{5}$$

The refractive index for the quasi-electrostatic model is given by:

$$\mu^2 = \frac{\lambda Y^2\left[\theta' \pm \left(\theta' - 2\alpha_{00}\beta\right)^{1/2}\right]}{\left[Y^2 - 1\right]^{1/2}\alpha_{00}\beta}, \tag{6}$$

where

$$\beta = \frac{\omega_p^2 T_e}{\omega_c^2 m_e c^2},$$

$$\alpha_{00} = \frac{Y^2\left(-11Y^2 + 23\right)}{\left(Y^2 - 1\right)^2\left(4Y^2 - 1\right)},$$

and where Y is defined as in the previous section and θ', defined as $\theta' = \theta - \theta_R$, where θ is the wave normal angle of the wave, θ_R is the cold plasma resonance cone angle given as:

$$\sin^2\theta_R = \frac{\left(1-\lambda Y^2\right)\left(1-Y^2\right)}{\lambda Y^4}. \tag{7}$$

The refractive index for the electrostatic model is given by:

$$\mu^2 = \frac{2\theta'\lambda Y^2}{\left[Y^2 - 1\right]^{1/2}\alpha_{00}\beta}. \tag{8}$$

Fig. 2 shows the refractive indices calculated using the warm plasma, quasi electrostatic and electrostatic approximations at $L=4$ for $\omega/\omega_c = 0.4$ plotted as a function of θ' near the resonance cone where the quasi-electrostatic and electrostatic models have validity and the cold plasma model does not produce a solution. For these oblique wave normal angles there is good agreement between the models. Electrostatic and quasi-electrostatic models agree perfectly when the wave normal angles are higher than the resonance cone angle ($\theta' > 0$). The electrostatic approximation does not provide a solution for $\theta' < 0$. The warm plasma model predicts slightly lower values of refractive index. The near perfect agreement between the electrostatic and quasi-electrostatic models is a feature for all cases considered here though these models give divergent results for higher frequencies near $\omega/\omega_c = 0.8$ [8].

Figs. 3 and 4 show the comparison results of refractive indices at L = 6 and 6.6 where the background density is lower. From the plots, a very close agreement between warm plasma assumptions and quasi-electrostatic approximations can be observed for $\theta' < \theta_R$. The warm plasma model again predicts slightly lower values of refractive index when $\theta' > 0$ and this is more pronounced for the L= 6.6 location.

Figs. 5-7 show the results obtained at the three selected locations for $\omega/\omega_c = 0.6$. In all figures, warm plasma approximations produce much higher refractive indices compared to the other two approximations.

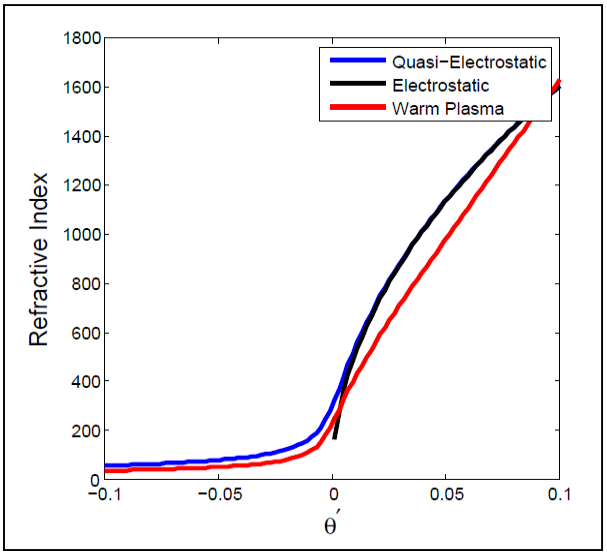

Fig. 2. Comparison of refractive index calculated with quasi-electrostatic, electrostatic and warm plasma models near the resonance cone (θ' = 0) for L = 4 (λ = 111) and $\omega/\omega_c = 0.4$.

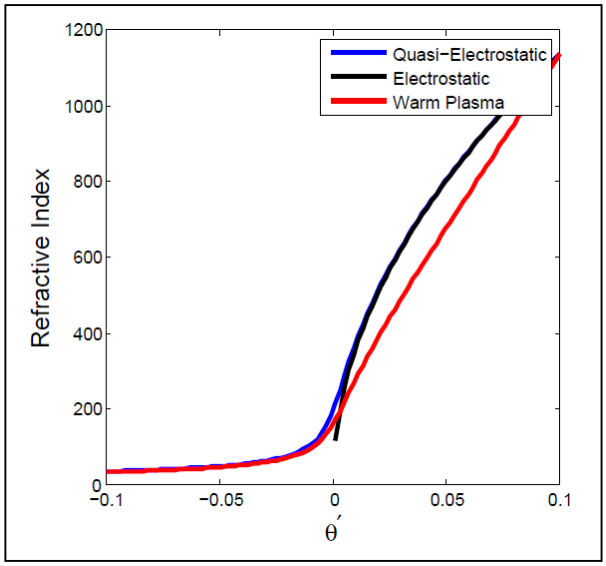

Fig. 3. Comparison of refractive index calculated with quasi-electrostatic, electrostatic and warm plasma models near the resonance cone (θ' = 0) for L = 6 (λ = 42.82) and ω/ω_c = 0.4 .

IV. Discussion

Horne and Sazhin [8], perform a comparison between quasi-electrostatic, electrostatic and what they call hot plasma assumptions that derive from the HOTRAY code [9]. Unfortunately, the details of the hot plasma formulations used for the comparison are not clear [8]. The electrostatic and quasi-electrostatic results shown here differ slightly from *Horne and Sazhin* [8] due to our neglect of the "hot" 200 eV population mentioned above. However, we note that our warm plasma results agree nearly exactly with the *Horne and Sazhin* [8] HOTRAY plasma results for $\omega/\omega_c = 0.4$ at L=4, L= 6. For $\omega/\omega_c = 0.4$ and L = 6.6 the agreement is still very good except that the HOTRAY results shows a discontinuity around the resonance cone angle. For the higher frequency cases $\omega/\omega_c = 0.6$ the warm plasma model produces higher refractive index values compared to the HOTRAY code. For the ratio $\frac{\omega}{\Omega} = 0.8$, the values obtained from the warm plasma assumptions are smaller than the values obtained from the HOTRAY code.

For frequencies below the half gyrofrequency, like the cases at $\omega/\omega_c = 0.4$ considered here, there is general agreement between the different models especially at the resonant cone angles and slightly smaller wave normal angles. Therefore, for analysis of oblique lower band chorus phenomena, especially at background densities of 200 cm^{-3} or higher, any of the models can be expected to provide reasonable results. At the same time, it is clear that for lower background densities and higher frequencies, the models discussed here do not show exact agreement. Specific knowledge of the hot plasma distribution and its density may be necessary for accurate estimates of the refractive index of highly oblique waves in such conditions.

One advantage of the warm plasma formulation presented here is that it provides solutions for all wave normal angles and reduces to the well-known cold plasma solutions for moderately oblique and field aligned waves. Using this formulation a robust raytracing code can be deployed to assess whistler mode trajectories and properties over the full scale of the magnetosphere. Such a raytracing code is presented by *Maxworth and Golkowski* [5]. It can be argued that a full hot plasma kinetic approach to raytracing is the most accurate and preferable approach. However, a full kinetic approach is computationally expensive.

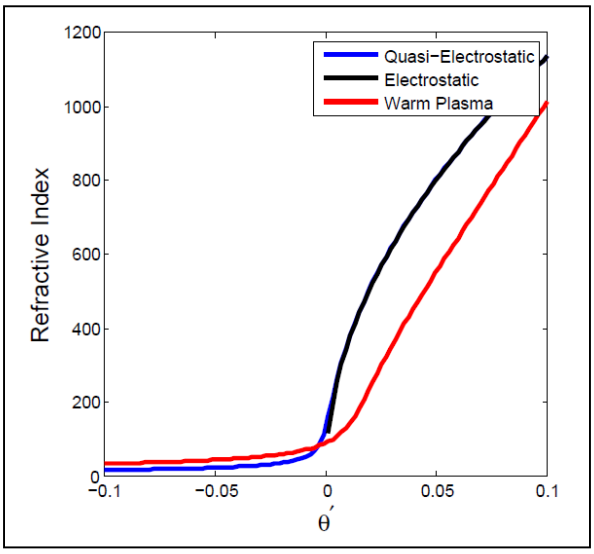

Fig. 4. Comparison of refractive index calculated with quasi-electrostatic, electrostatic and warm plasma models near the resonance cone (θ' = 0) for L = 6.6 (λ = 8.96) and ω/ω_c = 0.4 .

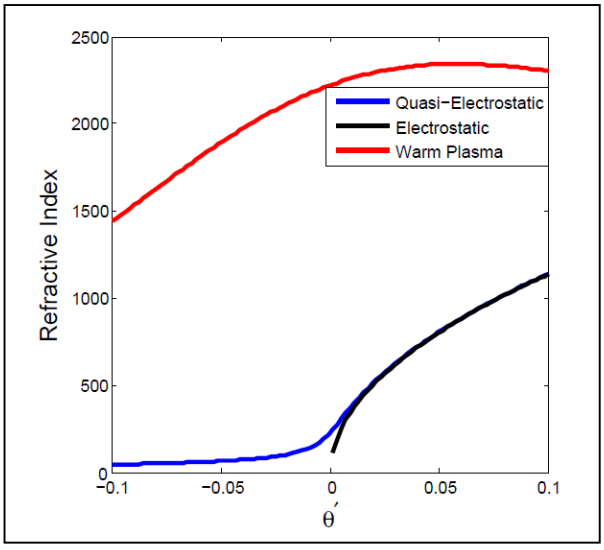

Fig. 5. Comparison of refractive index calculated with quasi-electrostatic, electrostatic and warm plasma models near the resonance cone (θ' = 0) for L = 4 (λ = 111.95) and ω/ω_c = 0.6 .

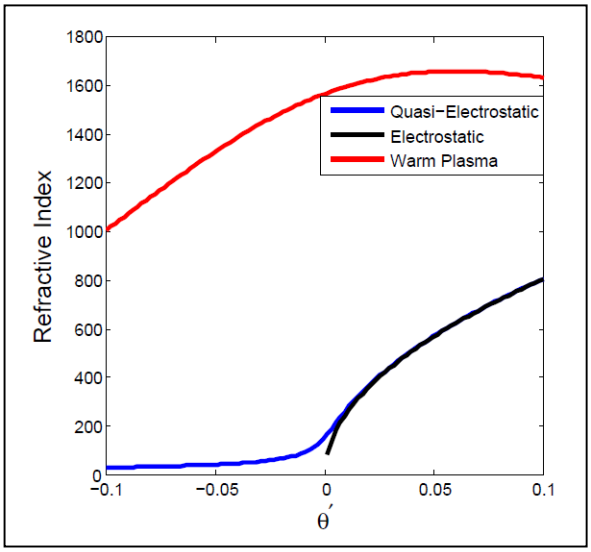

Fig. 6. Comparison of refractive index calculated with quasi-electrostatic, electrostatic and warm plasma models near the resonance cone (θ' = 0) for L = 6 ($\lambda = 42.82$) and $\omega/\omega_c = 0.6$.

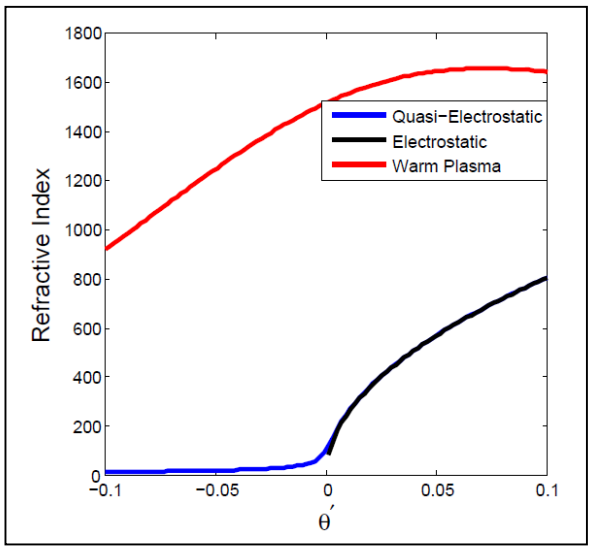

Fig. 7. Comparison of refractive index calculated with quasi-electrostatic, electrostatic and warm plasma models near the resonance cone (θ' = 0) for L = 6.6 ($\lambda = 8.96$) and $\omega/\omega_c = 0.6$.

V. Conclusions

Inclusion of finite temperature of the background plasma changes the refractive index for highly oblique whistler waves. Recent spacecraft observations show a significant presence of such highly oblique whistler mode waves and their role in radiation belt dynamics are still being assessed. A primary effort in space weather research is modeling energetic particle populations using quasi-linear diffusion codes. The upper limit of the refractive index surface has been identified as an important parameter [10]. So even if inclusion of finite temperature does not significantly change a typical whistler wave trajectory from that predicted by cold plasms theory, the implications of refractive index change at oblique wave normal angles can have far reaching effects. The warm plasma theory discussed here allows for calculation of the maximum refractive index outside the resonance cone. The warm plasma approach shows very similar results to quasi electrostatic and electrostatic approximations near the resonance cone for frequency below the half gyrofrequency making the model a robust choice for general whistler mode raytracing problems.

References

[1] U. S. Inan, S. Umran, and M. Gołkowski, Principles of Plasma Physics for Engineers and Scientists. Cambridge University Press, 2010.

[2] P. M. E Decreau, C. Beghin, and M. Parret, "Global characteristics f the cold plasma in the equatorial plasmasphere region as deduced from the GEOS 1 mutial impedance probe," J. Geophys. Res A87, 695, 1982.

[3] J. Haselgrove, "Ray theory and a new method for ray tracing," in Physics of the Ionosphere, Physics of the Ionosphere Conference, Cambridge, London, 355-364, 1954.

[4] P. Kulkarni, M. Gołkowski, U. S. Inan, and T. F. Bell, "The effect of electron and ion temperature on the refractive index surface of 1-10 kHz whistler mode waves in the inner magnetosphere," J. Geophys. Res. Space Physics, 120, 1, 581-591, 2015.

[5] A. S. Maxworth and M. Gołkowski, "Magnetospheric whistler mode raytracing in a warm background plasma with finite electron and ion temperature," J. Geophys. Res. Space Physics, 122, 7, 7323-7335, 2017.

[6] Q. Ma, et al., "Very oblique whistler mode propagation in the radiation belts: Effects of hot plasma and Landau damping," Geophys. Res. Lett., 2017.

[7] D. M Malaspina, et al., "The distribution of plasmaspheric hiss wave power with respect to plasmapause location," Geophys. Res. Lett., 43, 15, 7878-7886, 2016.

[8] R. B. Horne and S. S. Sazhin, "Quasielectrostatic and electrostatic approximations for whistler mode waves in the magnetospheric plasma," Planetary and Space Science, vol. 38, iss. 2, 1990.

[9] R. B. Horne "Path-integrated growth of electrostatic waves: The generation of terrestrial myriametric radiation," J. Geophys. Res., 94, A7, 8895-8909, 1989.

[10] J. M. Albert, "Quasi-linear diffusion coefficients for highly oblique whistler mode wave," J. Geophys. Res., 122, 5, 5339-5354, 2017.